Nanoscale

Accepted Manuscript

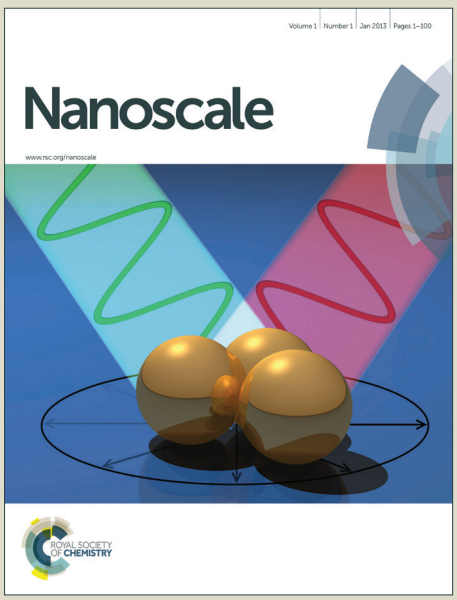

ROYAL SOCIETY OF CHEMISTRY

www.rsc.org/nanoscale

Cite this: DOI: 10.1039/c0xx00000x

www.rsc.org/xxxxxx

ARTICLE

Cellulose nanofibrils efficiently improve mechanical, thermal and oxygen-barrier properties of all-cellulose composites by nano-reinforcement mechanism and nanofibril-induced crystallization

Quanling Yang,[a] Tsuguyuki Saito,[a] Lars A. Berglund[b] and Akira Isogai*[a]

Received (in XXX, XXX) Xth XXXXXXXXX 20XX, Accepted Xth XXXXXXXXX 20XX
cDOI: 10.1039/b000000x

All-cellulose nanocomposite films containing crystalline TEMPO-oxidized cellulose nanofibril (TOCN) of 0–1 wt % were fabricated by mixing aqueous TOCN dispersions with alkali/urea/cellulose (AUC) solutions at room temperature. The mixtures were cast on glass plates, soaked in an acid solution, and the regenerated gel-like films were washed with water then dried. The TOCN did not form agglomerates in the composites, and had structures of TOCN–COOH, forming hydrogen bonds with the hydroxyl groups of the regenerated cellulose molecules. X-ray diffraction analysis revealed that the matrix cellulose molecules increased the cellulose II crystal size upon incorporation of TOCN. As a result, the TOCN/AUC composite films had high Young's modulus, tensile strength, thermal stability and oxygen-barrier properties. The TOCN/AUC composite films are promising all-cellulose nanocomposites for versatile applications as new bio-based materials.

Introduction

Plant celluloses are advantageous for use as bio-based, reproducible and carbon-neutral materials, which are required for a sustainable society. Celluloses used so far are classified into two groups. One includes fibrous native celluloses, mostly consisting of crystalline microfibrils as the smallest elements next to cellulose molecules; and the other involves regenerated or man-made celluloses, prepared by dissolution of native celluloses in a solvent followed by spinning or extrusion into a regeneration bath and drying. Fibrous native celluloses generally have high elastic moduli, tensile strengths and thermal dimensional stabilities, primarily owing to highly crystalline cellulose microfibrils, but have heterogeneous morphologies and limited sizes. Regenerated celluloses, on the other hand, have uniform fibrous and film-like morphologies with almost infinite lengths. Thus, regenerated cellulose fibers and films have been produced on large scales at the industrial level, and widely used as high-tech and ordinary materials.

Among the many cellulose solvent systems reported, the aqueous alkali/urea system is one of the most promising systems in terms of environmental considerations,[1] and thus may be able to partly replace the conventional viscose (i.e., aqueous $NaOH/CS_2$) system.[2,3] The preparation and characterization of various regenerated celluloses and related composites have been reported using the alkali/urea/cellulose (AUC) solutions, and some have exhibited unique and excellent properties.[4–7] Nanocelluloses have recently attracted attention as nano-sized and bio-based materials prepared from abundant biomass recourses. Nanocelluloses are roughly categorized as cellulose nanofibrils (CNFs) and cellulose nanocrystals (CNCs) with high and low aspect ratios, respectively.[8,9]

The preparation and characterization of all-cellulose composites consisting of plant cellulose fibers, CNFs or CNCs as fillers and regenerated celluloses or cellulose derivatives as matrices have been reported.[10–16] AUC solutions have been used to prepare all-cellulose composites consisting of regenerated cellulose as a matrix.[7,17–20] The mechanical properties and thermal stability of regenerated cellulose films were improved in most cases by forming a composite with a cellulose reinforcement. However, when cotton CNCs were used as fillers in regenerated cellulose films prepared from AUC solutions, the CNC contents of more than 10 wt % (based on the whole CNC and cellulose weight) were needed to achieve a Young's modulus double that of the original AUC films.[17,18] When fibrous native or regenerated cellulose was used as a filler, the films were opaque and their mechanical properties were not improved as efficiently,[4,19,20] owing to their heterogeneous morphologies and low aspect ratios.

Cellulose microfibrils present in plant cellulose fibers are firmly bound to each other through numerous hydrogen bonds; it has been difficult to convert plant cellulose fibers to individual nanocelluloses. Catalytic oxidation under aqueous conditions with 2,2,6,6-tetramethylpiperidinyl-1-oxyl (TEMPO) convert plant cellulose fibers to individual TEMPO-oxidized cellulose nanofibrils (TOCNs) with homogeneous widths of ~3 nm after gentle mechanical disintegration of TEMPO-oxidized cellulose (TOC) fibers in water.[21,22] Almost all of the C6-primary hydroxyl

groups exposed on the crystalline cellulose microfibril surfaces can be position-selectively converted to C6-carboxylate groups, when the TEMPO-mediated oxidation is applied to plant celluloses under suitable conditions.[23–25] Electric repulsions and osmotic forces effectively work between the surface-carboxylate cellulose microfibrils present in TOCs with carboxylate contents ≥ 1 mmol g^{-1} in water, resulting in TOCNs with ~3 nm widths and high aspect ratios (> 100). TOCNs thus obtained have high elastic moduli of ~134 GPa[26] and high tensile strengths of ~3 GPa.[27] The TOCN aerogels have large specific surface areas of ~800 m^2 g^{-1}, and the TOCN cast films have high oxygen-barrier properties and coefficients of thermal expansion of 0–6 ppm K^{-1}.[28–30] Thus, the TOCNs are promising bio-based nanomaterials for use as nanofillers in polymer matrices.[31]

In this study, we fabricated transparent all-cellulose nanocomposite films consisting of TOCN (≤ 1 wt %) and regenerated cellulose as the reinforcement and matrix components, respectively. Aqueous TOCN dispersions and AUC solutions were used to prepare the TOCN/AUC composite films. The TOCN nano-reinforcing effects were evaluated by measuring optical, mechanical, thermal and oxygen-barrier properties of the composite films.

Experimental

Materials

A highly purified cotton linters pulp (filter paper pulp; Advantec Co. Ltd., Tokyo, Japan) was used as cellulose to prepare AUC solutions. A never-dried softwood bleached kraft pulp (SBKP) (Nippon Paper Ind. Co., Tokyo, Japan), which contained ~90% α-cellulose and ~10% hemicelluloses, was used to prepare TOC and TOCN dispersions. All reagents and solvents were of laboratory grade and used as received from Wako Pure Chemicals, Tokyo, Japan.

Preparation of AUC solution and aqueous TOCN dispersion

A NaOH/urea/H_2O solution with a weight ratio of 7:12:81 was precooled to –12 °C.[5] The cotton linters cellulose was dispersed in the solvent, and the mixture was immediately stirred at 1,300 rpm for 2 min at the same temperature to obtain a transparent AUC solution with a 4 wt % cellulose concentration. A fibrous TOC was prepared from SBKP by the TEMPO/NaBr/NaClO system with 3.8 mmol NaClO per gram of SBKP in water at pH 10, according to a previously reported method.[21,32] The fibrous TOC was further treated with 1 w/v % $NaClO_2$ in water at pH 4.8 and room temperature for 2 days to oxidize the TOC C6-aldehydes to C6-carboxyls.[32] This $NaClO_2$-treated TOC had a carboxylate content of 1.21 mmol g^{-1}, as determined by the conductivity titration method.[21–24,32] A 0.1 w/v % $NaClO_2$-treated TOC/water slurry was mechanically disintegrated to prepare a transparent and highly viscous TOCN dispersion, according to a previously reported method.[29–32]

Preparation of TOCN–COONa and TOCN–COOH films

The TOCN film with sodium carboxylate groups (TOCN–COONa) was prepared by casting the TOCN dispersion on a petri dish and drying in an oven at 40 °C for 3 days.[28,29] The TOCN film with protonated carboxyl groups (TOCN–COOH) was prepared from the aqueous TOCN dispersion by addition of a dilute HCl solution and successive disintegration treatments, according to a previously reported method.[33]

Preparation of TOCN/AUC composite films

The scheme to fabricate TOCN/AUC composite films is provided in Figure 1. A designed amount of the TOCN dispersion was slowly added to the AUC solution at room temperature with continuous stirring, and the mixture was stirred for 30 min. The TOCN-containing AUC solution was then cast on a glass plate and soaked in 5 wt % aqueous H_2SO_4 for 5 min. The regenerated TOCN/AUC composite gel was washed thoroughly with water, and air-dried at 23 °C and 50% relative humidity (RH) for more than 1 day to obtain TOCN/AUC composite films. The soaking, washing and drying conditions to prepare TOCN/AUC films were the same as those for the preparation of AUC films.[5] The TOCN contents in the composite films were controlled to 0.2, 0.4, 0.6, 0.8, and 1.0 wt %, and these films were named as TOCN–0.2/AUC, TOCN–0.4/AUC, TOCN–0.6/AUC, TOCN–0.8/AUC and TOCN–1.0/AUC, respectively.

Analyses

The surface morphology of the TOCN films was observed by atomic force microscopy (AFM) using a Nanoscope IIIa controller (Veeco Instruments Inc., USA) operated in tapping mode with a silicon nitride cantilever tip. The TOCN dispersion was diluted to 0.002 w/v % with water, dropped onto a mica plate, and oven-dried before AFM observation. Fourier transform infrared (FTIR) spectra of the films were recorded using a Jasco FT/IR-6100 spectrometer under transmission mode from 400 to 4000 cm^{-1} with a 4 cm^{-1} resolution. X-ray diffraction (XRD) patterns of the films were acquired in reflection mode using a RINT 2000 diffractometer (Rigaku, Tokyo, Japan) with monochromator-filtered Cu Kα radiation (λ=0.15418 nm) at 40 kV and 40 mA. The crystal size of cellulose II was calculated from the full-width-at-half-height of the (1 –1 0) diffraction peak using the Scherrer equation.[34] The surface and cross-section (fracture surface) of the films were coated with osmium using a Meiwafosis Neo osmium coater at 10 mA for 10 s, and observed with a Hitachi S4800 field-emission-type scanning electron microscope (SEM) at 2 kV. The optical transmittance of the films was measured from 200 to 800 nm with a Shimadzu UV-1700 UV-Vis spectrophotometer. Tensile tests were performed using a Shimadzu EZ-TEST instrument equipped with a 500 N load cell. Rectangular strips with dimensions of 2×30 mm^2 were cut from the composite films and tested with a span length of 10 mm at a rate of 1.0 mm min^{-1}. The thermal expansivity of the films, which were preheated at 120 °C for 10 min, was determined using a 0.03 N load cell in a nitrogen atmosphere from 28 to 100 °C at 5 °C min^{-1} with a Shimadzu TMA-60 instrument. The film thickness was measured with a micrometer and each value was expressed as an average of five measurements. Statistical errors in thickness of each film were within ±3%. The oxygen transmission rate of the composite films was determined at 23 °C using a Mocon Ox-Tran Model 2/21MH (Modern Controls Inc., USA) under standard conditions (ASTM 3985). Each measurement was continued until the O_2 transmission rate reached a stable value. The oxygen permeability was determined from the oxygen transmission rate and the film thickness.

Results and discussion

Fabrication of TOCN/AUC composite films

To ensure that the TOCNs were fully nano-dispersed in the AUC solution without dissolution, the mixture was stirred at room temperature for 30 min (Figure 1). No further changes in the mechanical and optical properties of the composite films were observed when the mixture was stirred for 1 h. Thus, we infer that the TOCNs were stable in the alkaline AUC solution at room temperature and the original cellulose I crystal structure was also maintained, as discussed later.

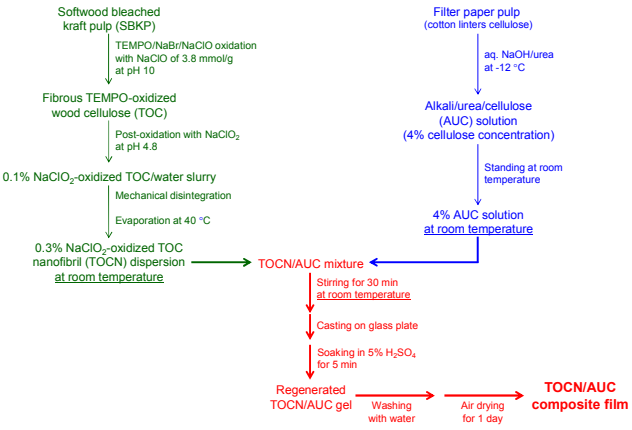

Fig. 1 Fabrication scheme of TOCN/AUC composite films from aqueous TEMPO-oxidized wood cellulose nanofibril (TOCN) dispersion and cotton linters cellulose/alkali/urea solution.

Figure S1 in the Supplementary Information shows an AFM image of the TOCN, which shows mostly individual TOCNs. The number-average TOCN length, measured and calculated from 50 TOCNs, and was 1158 ± 421 nm. The number-average TOCN width was determined from AFM height profiles of 50 TOCN according to a previously reported method,[27] and was 2.7 ± 0.3 nm. Thus, the TOCN exhibits a high average aspect ratio of ~430. The small widths and high aspect ratios of the TOCNs are expected to contribute to enhanced nano-reinforcing effects for composites, as long as TOCNs disperse in the matrix without agglomeration.[35] It is unknown at present whether the TOCN bending points in Figure S1 exist in the aqueous dispersion state or form during the drying process of the TOCN dispersion on the mica plate for AFM observation.

Optical properties and SEM observations of TOCN/AUC composite films

Figure 2 shows the light transmittance spectra of the composite films and a photograph of the TOCN–1.0/AUC film. All of the TOCN/AUC films were transparent and flexible. The light transmittances of the TOCN/AUC films were higher than 88% at 600 nm, which is sufficient for application as film materials such as display panels, electronic devices, and high performance packaging films for foods and medicines. These light transparencies were higher than those (< 80%) of the other all-cellulose composite films containing native or regenerated cellulose fibres as fillers, when compared with the same film thickness of 30 μm.[4,19] The high light transparency was indicative of good TOCN nano-dispersibility in the AUC matrix.[36] The slight decrease of light transmittance for the TOCN/AUC composite films is probably caused by light scattering at the TOCN/AUC interfaces.

The SEM images of surfaces and cross-sections of AUC and TOCN–1.0/AUC films are shown in Figure S2 in the Supplementary Information. These films had homogenous and similar surfaces, and the TOCN–1.0/AUC film showed no obvious TOCN agglomerates. The film cross-sections showed laminated structures. We infer that these result from the in-plane orientation of the crystalline regenerated cellulose molecules and TOCN during the TOCN/AUC film dying process. The results shown in Figures 2 and S1 indicate that TOCNs are present individually without agglomeration, and that the TOCN and regenerated cellulose molecules have good compatibility in both aqueous TOCN/AUC mixtures and dried TOCN/AUC composite films. The orientation of cellulose II crystallites in the TOCN–1.0/AUC film was further studied for the film cross-section by two-dimensional X-ray diffraction analysis (Figure S3 in the Supplementary Information). The strong arc diffractions due to (1 –1 0), (1 1 0) and (0 2 0) planes were observed, showing that the longitudinal direction of cellulose II crystallites were highly oriented parallel to the film surface. The Herman's orientation parameter (f)[37] of the cellulose II crystallites was calculated to be 0.85 from the X-ray diffraction pattern of this film.

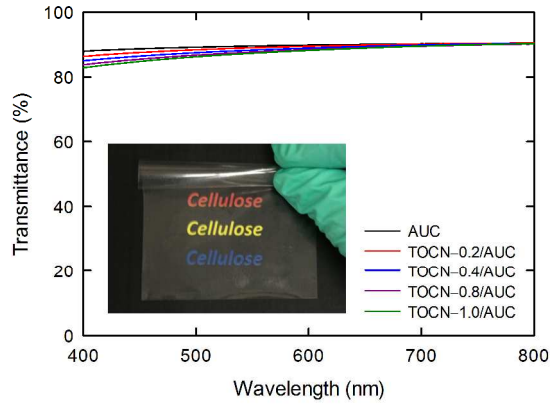

Fig. 2 Light transmittance spectra of TOCN/AUC composite films with thickness of 30 μm and a photograph of the TOCN–1.0/AUC film.

Interactions between TOCN and regenerated cellulose molecules in composite films

FTIR measurements were performed on the films to study the interactions between TOCN and regenerated cellulose molecules (Figure 3). The large absorption band at 3000–3600 cm^{-1} in the AUC film is due to the hydroxyl groups from cellulose and water adsorbed on the film. The band at ~1640 cm^{-1} is assigned to water molecules.[33] The TOCN–COONa film had an absorption band at ~1607 cm^{-1} owing to C=O stretching of carboxylate groups.[33] The TOCN–COOH film had an absorption band at ~1724 cm^{-1} due to C=O stretching of protonated carboxyl groups, forming hydrogen bonds between two carboxyl groups.[33] It has been reported that isolated carboxyl groups without forming any hydrogen bonds exhibit a C=O stretching band at ~1740 cm^{-1}.[38–

[41] The TOCN/AUC films had a C=O stretching band at ~1732 cm^{-1}, showing that the carboxyl groups in the film had protonated structures. Thus, the sodium carboxylate structures of TOCN–COONa changed to protonated TOCN–COOH structures in the TOCN/AUC films during the regeneration process of the TOCN/AUC mixtures by soaking in 5 wt % H_2SO_4.

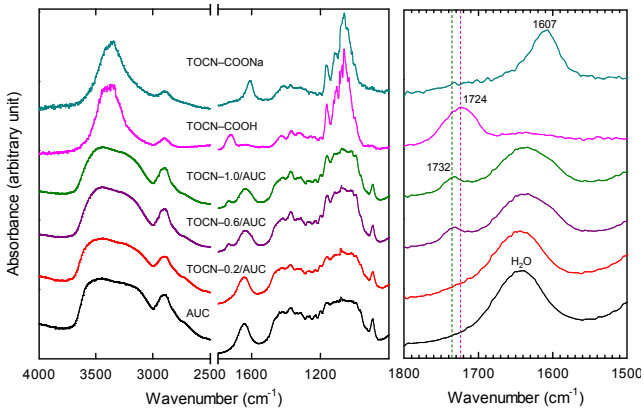

Fig. 3 FTIR spectra of AUC, TOCN–COONa, TOCN–COOH and TOCN/AUC composite films.

The C=O stretching bands with and without hydrogen bonds between two carboxyl groups appear at 1724 and 1740 cm^{-1}, respectively.[38–41] The C=O stretching band of the TOCN/AUC films appeared at ~1732 cm^{-1}, which is intermediate between 1724 and 1740 cm^{-1}. We infer that each TOCN protonated carboxyl group forms a hydrogen bond with one or two hydroxyl groups of the regenerated cellulose molecules in the TOCN/AUC composite films without forming TOCN/TOCN hydrogen bonds. The formation of hydrogen bonds between carboxyl groups of TOCN–COOH and hydroxyl groups of the AUC matrix have a positive influence on enhancing the mechanical properties of the composite films, as discussed later.

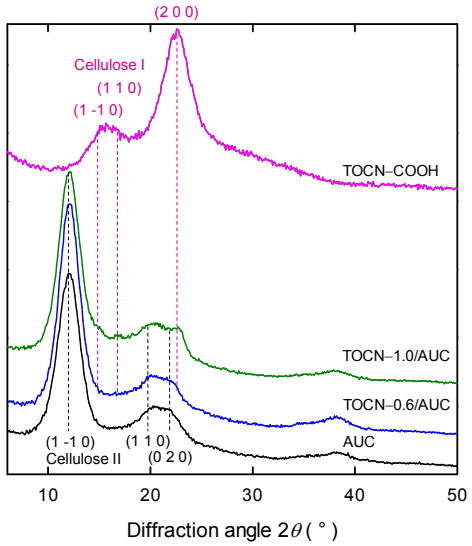

Fig. 4 XRD patterns of AUC, TOCN–COOH and TOCN/AUC composite films.

The XRD patterns of AUC, TOCN and TOCN/AUC composite films are shown in Figure 4. The AUC film showed a cellulose II crystal pattern with clear orientation of the (1 –1 0) plane parallel to the film surface.[5] In contrast, the TOCN film showed a cellulose I crystal pattern, maintaining the original crystal structure of native wood cellulose. The TOCN/AUC composite films showed clear diffraction peaks of cellulose II as a dominant component of crystalline regenerated cellulose molecules. Small diffraction peaks of (1 1 0) and (2 0 0) of cellulose I originating from the TOCN were detected in the XRD pattern of the TOCN–1.0/AUC film.

It is noteworthy that the relative crystal size of cellulose II calculated from the (1 –1 0) peak slightly increased from 3.4 nm to 3.7 nm by incorporation of 1 wt % TOCN. These results indicate that AUC molecules in the films increased in the amount of ordered structures by incorporation of crystalline TOCNs with high aspect ratios. The hydrogen bond formation between TOCN and regenerated cellulose molecules (cf. Figure 3) may have resulted in the increase in crystal size of cellulose II of cellulose molecules in the composite films. Similar results were observed for highly drawn TOCN/poly(vinyl alcohol) composite fibers.[42]

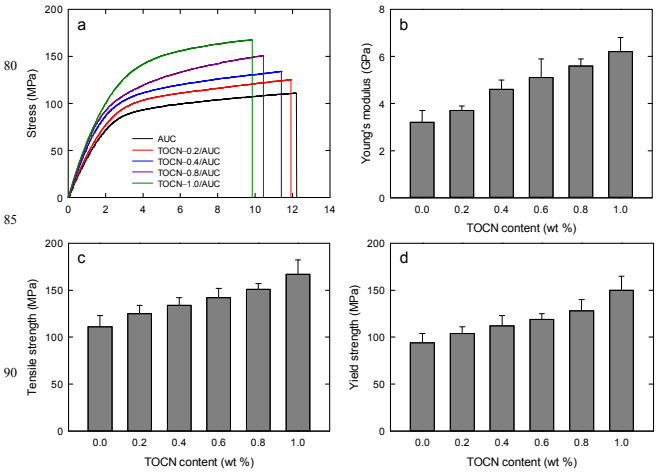

Fig. 5 Stress-strain curves (a) and effects of the TOCN content on Young's modulus (b), tensile strength (c), and yield strength (d) of the AUC-only and TOCN/AUC composite films.

Mechanical properties of TOCN/AUC composite films

The stress-strain curves and the effects of TOCN content on Young's modulus, tensile strength and yield strength of the TOCN/AUC composite films are shown in Figure 5. The stress-strain curve of the AUC film consisted of two phases: the initial elastic region followed by a large plastic region. The TOCN/AUC composite films also exhibited curves consisting of two phases, but the ratio of elastic region increased with increasing the TOCN content, owing to the high elastic modulus of TOCN.[26]

The Young's modulus, tensile strength and yield strength clearly increased with incorporation of small amounts of TOCN into the AUC films. As the TOCN content increased from 0 to 1 wt %, Young's modulus increased from 3.2 to 6.2 GPa, the tensile strength increased from 111 to 167 MPa, and the yield strength increased from 94 to 150 MPa. The elongation at break slightly decreased from 12% to 10%, and the work of fracture increased slightly from 11 to 13 MJ m^{-3}. The increase in Young's modulus and tensile strength or the efficient increases in the mechanical properties were achieved by incorporation of high

aspect ratio TOCN without agglomeration in the AUC matrix.

Several prediction methods of mechanical properties for fiber/matrix composites have been proposed on the basis of theoretical models to evaluate the validity of the fiber reinforcement.[43] Figure 6 shows the experimentally obtained and calculated Young's moduli (top) and tensile strengths (bottom) of the TOCN/AUC composite films. When the Young's modulus and tensile strength of 3.2 GPa and 111 MPa, respectively, experimentally obtained for the neat AUC film were used as constant values for the AUC matrix, the experimentally obtained Young's modulus and tensile strength of the TOCN/AUC composite films were always higher than those calculated using the Halpin-Tsai model (see Supplementary Information).[43] However, when the Young's moduli of the AUC matrix (cf. Fig. S4) were assumed to increase to 3.7, 4.2, 4.8, 5.3 and 5.8 GPa in the TOCN–0.2/AUC, TOCN–0.4/AUC, TOCN–0.6/AUC, TOCN–0.8/AUC and TOCN–1.0/AUC composites, respectively, the experimentally obtained Young's moduli of the nanocomposite films were well consistent with those calculated using the modified model.

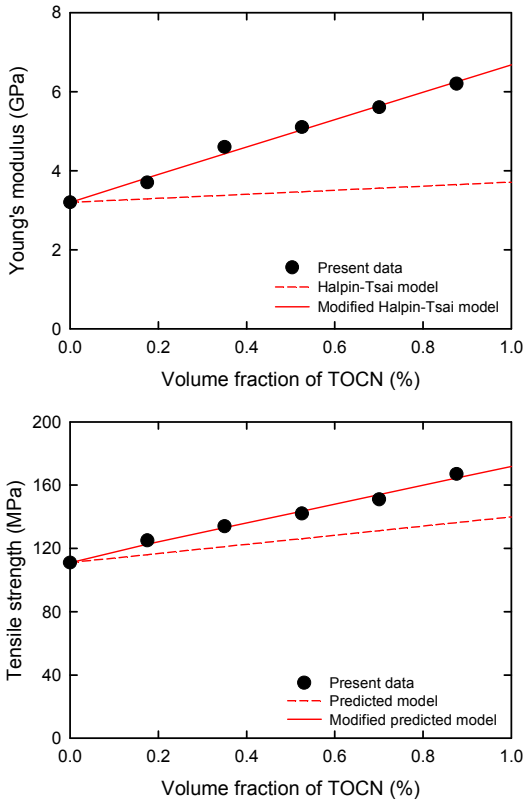

Fig. 6 Effects of volume fractions of TOCNs on experimentally obtained and calculated Young's modulus (top) and tensile strength (bottom) of the TOCN/AUC composite films (see Supplementary Information).

Similar results were obtained also for the relationship between the experimentally obtained tensile strengths and those calculated using the modified model, although this is a rough and empirical estimate. When the tensile strength of the AUC matrix were assumed to increase to 118, 123, 128, 134 and 139 MPa in the TOCN–0.2/AUC, TOCN–0.4/AUC, TOCN–0.6/AUC, TOCN–0.8/AUC and TOCN–1.0/AUC composites, respectively, the experimental data were consistent with those calculated using the modified models. The efficiency to improve tensile strength of AUC films by compositing TOCNs shown in the present work was much higher than those for the previously reported CNC/AUC composite films, when compared at the same nanocellulose volume fraction.[17,18] Thus, the incorporation of TOCNs in AUC molecules caused the increases in Young's modulus and tensile strength of the AUC matrix, resulting in the high mechanical properties of the TOCN/AUC composites.

In the previous section, it was shown from the XRD data in Figure 4 that the regenerated cellulose molecules increased in the cellulose II crystal size with the incorporation of crystalline TOCNs with high aspect ratios into the AUC film. The regenerated cellulose molecules next to each TOCN are likely to form favourable morphologies with molecular orientation along the TOCN, which might be regarded as a unique nucleation effect. Thus, the increase in the cellulose II crystal size of the AUC matrix molecules with increasing the TOCN content is associated with the increased crystalline order and high mechanical properties of TOCN, resulting in the efficient increases in the Young's modulus and tensile strength of the composite films.

Thermal stability and oxygen barrier property of TOCN/AUC composite films

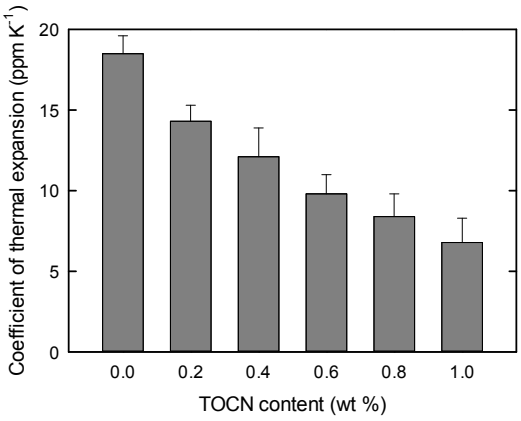

Fig. 7 Effect of TOCN content on the coefficient of thermal expansion of TOCN/AUC composite films.

The coefficients of thermal expansion (CTEs) of the TOCN/AUC composite films were determined to evaluate their dimensional stability (Figure 7). As the TOCN content was increased from 0 to 1.0 wt %, the CTE value decreased from 18.5 to 6.8 ppm K^{-1}. This CTE value of the TOCN–1.0/AUC film is similar to that of iron (~11.8 ppm K^{-1}), and much lower than those of most plastics (> 50 ppm K^{-1}).[44] Therefore, the TOCN/AUC composite films possessed excellent thermal-dimensional stability, owing to 1) the incorporation of crystalline TOCN, 2) the hydrogen bonds between the TOCN and regenerated cellulose molecules, and 3) the increase in cellulose II crystal size of regenerated cellulose molecules in the composite films. Note that such low CTEs were observed only for once-dried TOCN/AUC composite films. When the films containing adsorbed water prepared under conditions at 50% RH were tested,

the films shrank upon heating and drying.

High oxygen-barrier properties are required for films used in display panels, electronic devices and high-performance packaging materials. The bulk TOCN–COONa films and nanoclay-containing TOCN–COONa films had oxygen transmittance rates lower than the detection limit of the standard instrument under dry conditions.[44,45] However, these values increased with increasing RH, owing to the hydrophilic nature of TOCN–COONa. In the case of the AUC-only and TOCN/AUC films, high oxygen barrier properties at 0% RH were observed, but the values increased with increasing RH, owing to the hydrophilic nature of regenerated cellulose molecules and TOCN in the composite films (Figure 8). The TOCN–1.0/AUC composite film clearly showed a lower oxygen permeability than that of the AUC-only film at the same RH. Compared with commercial polymer high oxygen-barrier films,[46] the oxygen permeabilities of the AUC-only and TOCN/AUC composite films at 50% RH were much lower than that of high-density poly(ethylene) or poly(ethylene terephthalate) films, and slightly lower than those of poly(vinylidene chloride) and poly(vinyl alcohol) films.

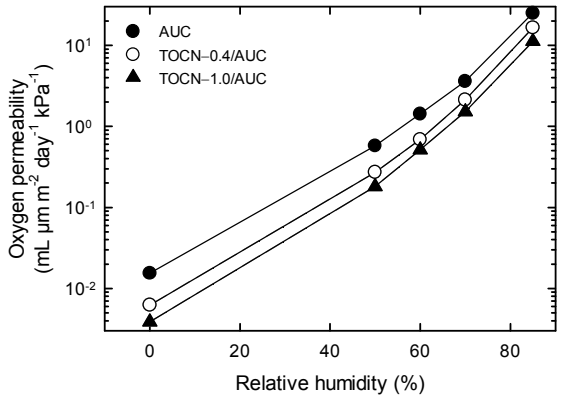

Fig. 8 Oxygen permeability of AUC-only and TOCN/AUC composite films at 0–90% RH.

Conclusions

The cellulose nanofibril/regenerated cellulose composite films, that is, all-cellulose nanocomposites, were fabricated from aqueous TOCN dispersion and aqueous AUC solution by mixing them at room temperature. The original structure of TOCN–COONa is converted to TOCN–COOH in the composite films during regeneration process of cellulose in acidic water, maintaining the original cellulose I crystal structure of wood cellulose. Hydrogen bond formation occurs between the TOCN and regenerated cellulose molecules, and the cellulose II crystal size of regenerated cellulose molecules increases in the composite films. This increase in the cellulose II crystal size, and associated effects when cellulose II is solidified in the presence of TOCNs, have resulted in a remarkable increase in effective Young's modulus and tensile strength of the AUC matrix in the composite film. As a result, the high mechanical performances of the crystalline TOCN and the TOCN-induced increases in crystal sizes of AUC matrix molecules resulted in the high Young's moduli and tensile strengths, and high oxygen-barrier properties and low CTEs at 0% RH for the TOCN/AUC composite films. These nanocomposite effects appear on the TOCN/AUC composite films, even though the TOCN contents are as low as only 1%.

Notes

[a]*Department of Biomaterials Science, The University of Tokyo, 1-1-1 Yayoi, Bunkyo-ku, Tokyo 113-8657, Japan. E-mail: aisogai@mail.ecc.u-tokyo.ac.jp*
[b]*Wallenberg Wood Science Centre, KTH Royal Institute of Technology, SE-10044 Stockholm, Sweden*

† Electronic Supplementary Information (ESI) available: Figures S1, S2 and S3 show an AFM image of TOCN, SEM images of the films, and the assumed Young's modulus and tensile strength of the AUC matrix in the composites. Models for prediction of Young's modulus and tensile strength of the composite films are summarized. See DOI: 10.1039/b000000x/

Acknowledgments

This study was supported by Core Research for Evolutional Science and Technology (CREST) of the Japan Science and Technology Agency (JST) and by the Japan Society for the Promotion of Science (JSPS): Grant-in-Aid for Scientific Research S (21228007) and Postdoctoral Fellowship for Foreign Researchers for QY (Grant P13392).

References

1 J. Cai, L. Zhang, J. Zhou, H. Qi, H. Chen, T. Kondo, X. Chen and B. Chu, *Adv. Mater.*, 2007, **19**, 821–825.
2 J. Cai and L. Zhang, *Macromol. Biosci.*, 2005, **5**, 539–548.
3 H. P. Fink, J. Ganster and A. Lehmann, *Cellulose*, 2014, **21**, 31–51.
4 Q. Yang, A. Lue and L. Zhang, *Compos. Sci. Technol.*, 2010, **70**, 2319–2324.
5 Q. Yang, H. Fukuzumi, T. Saito, A. Isogai and L. Zhang, *Biomacromolecules*, 2011, **12**, 2766–2771.
6 Z. Shi, H. Gao, J. Feng, B. Ding, X. Cao, S. Kuga, Y. Wang, L. Zhang and J. Cai, *Angew. Chem. Int. Ed.*, 2014, **53**, 5380 –5384.
7 Q. Yang, C. Wu, T. Saito and A. Isogai, *Carbohydr. Polym.*, 2014, **100**, 179–184.
8 D. Klemm, F. Kramer, S. Moritz, T. Lindström, M. Ankerfors, D. Gray and A. Dorris, *Angew. Chem. Int. Ed.*, 2011, **50**, 5438–5466.
9 A. Isogai, *J. Wood. Sci.*, 2013, **59**, 449–459..
10 T. Huber, J. Müssig, O. Curnow, S. Pang, S. Bickerton and M. P. Staiger. *J. Mater. Sci.*, 2012, **47**, 1171–1186.
11 H. Yousefi, T. Nishino, M. Faezipour, G. Ebrahimi and A. Shakeri, *Biomacromolecules*, 2011, **12**, 4080–4085.
12 H. Nilsson, S. Galland, P. T. Larsson, E. K. Gamstedt, T. Nishino, L. A. Berglund and T. Iversen, *Compos. Sci. Technol.*, 2010, **70**, 1704–1712.
13 T. Pullawan, A. N. Wilkinson and S. J. Eichhorn, *Compos. Sci. Technol.*, 2010, **70**, 2325–2330.
14 T. Huber, S. Bickerton, J. Müssig, S. Pang and M. P. Staiger, *Compos. Sci. Technol.*, 2013, **88**, 92–98.
15 J. Zhao, X. He, Y. Wang, W. Zhang, X. Zhang, X. Zhang,Y. Deng and C. Lu, *Carbohydr. Polym.*, 2014, **104**, 143–150.
16 T. Nishino, I. Matsuda and K. Hirao, *Macromolecules*, 2004, **37**, 7683–7687.
17 H. Qi, J. Cai, L. N. Zhang and S. Kuga, *Biomacromolecules*, 2009, **10**, 1597–1602.
18 T. Pullawan, A. N. Wilkinson, L. N. Zhang and S. J. Eichhorn, *Carbohydr. Polym.*, 2014, **100**, 31– 39.
19 A. V. Nadhan, A. V. Rajulu, R. Li, C. Jie and L. Zhang, *J. Polym. Environ.*, 2012, **20**, 454–458.
20 J. Jayaramudu, G. S. M. Reddy, K. Varaprasad, E. R. Sadiku, S. S. Ray and A. V. Rajulu, *Carbohydr. Polym.*, 2013, **93**, 622–627.
21 T. Saito, S. Kimura, Y. Nishiyama and A. Isogai, 2007, **8**, 2485–2491.
22 T. Saito, M. Hirota, N. Tamura, S. Kimura, H. Fukuzumi, L. Heux and A. Isogai, *Biomacromolecules*, 2009, **10**, 1992–1996.

23 M. Hirota, K. Furihata, T. Saito, T. Kawada and A. Isogai, *Angew. Chem. Int. Ed.*, 2010, **49**, 7670–7672.
24 Y. Okita, T. Saito and A. Isogai, *Biomacromolecles*, 2010, **11**, 1696–1700.
25 A. Isogai, T. Saito and H. Fukuzumi, *Nanoscale*, 2011, **3**, 71−85.
26 I. Sakurada, Y. Nukushima and T. Ito, *J. Polym. Sci.*, 1962, **57**, 651−660.
27 T. Saito, R. Kuramae, J. Wohlert, L. A. Berglund and A. Isogai, *Biomacromolecules*, 2013, **14**, 248−253.
28 H. Fukuzumi, T. Saito, Y. Kumamoto, T. Iwata and A. Isogai, *Biomacromolecules*, 2009, **10**, 162–165.
29 T. Saito, T. Uematsu, S. Kimura, T. Enomae and A. Isogai, *Soft Matter*, 2011, **7**, 8804–8809.
30 Y. Kobayashi, T. Saito and A. Isogai, *Angew. Chem. Int. Ed.*, 2014, **53**, 10394–10397.
31 S. Fujisawa, T. Saito, S. Kimura, T. Iwata and A. Isogai, *Biomacromolecules*, 2013, **14**, 1541−1546.
32 R. Shinoda, T. Saito, Y. Okita and A. Isogai, *Biomacromolecules*, 2012, **13**, 842−849.
33 S. Fujisawa, Y. Okita, H. Fukuzumi, T. Saito and A. Isogai, *Carbohydr. Polym.*, 2011, **84**, 579–583.
34 L. E. Alexander, X-ray diffraction methods in polymer science, 1979, Robert E. Kreiger Publishing Co., Humington, pp 423–424.
35 D. R. Paul and L. M. Robeson, *Polymer*, 2008, **49**, 3187–3204.
36 S. Krause, *J. Macromol. Sci. Macromol. Chem.*, 1972, **2**, 251–314.
37 H. Sehaqui, N. Mushi, S. Morimune, M. Salajkova, T. Nishino and L. A. Berglund, *ACS Appl. Mater. Interaces.*, 2012, **4**, 1043–1049.
38 R. V. Dueval and R. M. Corn, *Anal. Chem.*, 1992, **64**, 337–342.
39 E. L. Smith, C. A. Alves, J. W. Anderegg and M. D. Porter, *Langmuir*, 1992, **8**, 2707–2714.
40 L. Sun and R. M. Crooks, *Langmuir*, 1993, **9**, 1775–1780.
41 S. E. Creager and C. M. Steiger, *Langmuir*, 1995, **11**, 1852–1854.
42 R. Endo, T. Saito and A. Isogai, *Polymer*, 2013, **54**, 935–941.
43 R. Guzmán de Villoria and A. Miravete, *Acta Matter.*, 2007, **55**, 3025–3031.
44 H. Fukuzumi, T. Saito, S. Iwamoto, Y. Kumamoto, T. Ohdaira, R. Suzuki and A. Isogai, *Biomacromolecules*, 2011, **12**, 4057–4062.
45 C.-N. Wu, Q. Yang, M. Takeuchi, T. Saito and A. Isogai, *Nanoscale*, 2014, **6**, 392–399.
46 K. Miller and J. Krochta, *Trends Food Sci. Tech.*, 1997, **8**, 228–237.